DLP printing of non-modified protein-only compositions

Ayelet Bunin[+], Orit Harari-Steinberg[+], Doron Kam, Tatyana Kuperman, Moran Friedman-Gohas, Bruria Shalmon, Liraz Larush, Shay I. Duvdevani[+], Shlomo Magdassi**

A. Bunin, D.Kam, L.Larush, S. Magdassi

Institute of Chemistry and Center for Nanoscience and Nanotechnology, The Hebrew University of Jerusalem, Jerusalem 9190401, Israel.

E-mail: Shlomo.Magdassi@mail.huji.ac.il

O. Harari-Steinberg, T.Kuperman ,M.Friedman-Gohas

Tissue Engineering Research Laboratory, Sheba Medical Center, Tel Hashomer, Ramat-Gan, Israel.

B. Shalmon

Pathology Clinical Departments, Sheba Medical Center, Israel.

S.I. Duvdevani

Tissue Engineering Research Laboratory, Sheba Medical Center, Tel Hashomer, Ramat-Gan, Israel.

Department of Otorhinolaryngology, Head and Neck Surgery, Sheba Medical Center, Israel.

Sackler Faculty of Medicine, Tel Aviv University, Israel.

E-mail: Shay.duvdevani@sheba.health.gov.il

[+]These authors contributed equally to this work.

[*]Corresponding authors.

Keywords: 3D printing, digital light processing (DLP), non-modified, di-tyrosine, cell-laden

Abstract

This study explores the utilization of digital light processing (DLP) printing to fabricate complex structures using native gelatin as the sole structural component for applications in

biological implants. Unlike approaches relying on synthetic materials or chemically modified biopolymers, this research harnesses the inherent properties of gelatin to create biocompatible structures. The printing process is based on a crosslinking mechanism using a di-tyrosine formation initiated by visible light irradiation. Formulations containing gelatin were found to be printable at the maximum documented concentration of 30 wt.%, thus allowing the fabrication of overhanging objects and open embedded tubes with a compressive modulus akin to soft tissues. Cell adhesion and growth onto and within the gelatin-based 3D constructs were evaluated by examining two implant fabrication techniques: (1) cell seeding onto the printed scaffold and (2) printing compositions that contain cells (cell-laden). The preliminary biological experiments indicate that both the cell-seeding and cell-laden strategies enable making 3D cultures of chondrocytes within the gelatin constructs. This study underscores the potential of utilizing non-modified protein-only bioinks in DLP printing to produce intricate 3D objects with high fidelity, paving the way for advancements in regenerative tissue engineering.

1. Introduction

3D bioprinting holds great promise in the field of personalized medicine, including the fabrication of medical implants.[1] There are two main approaches to fabricating biological implants: printing a bio-scaffold followed by cell-seeding or printing compositions containing living cells (cell-laden).[2,3] The most common 3D bioprinting technology is based on Direct Ink Writing (DIW), in which the object is formed by extrusion. This technology is widely used due to the relatively low cost of printers and the ease of the printing process, while the ink could be made, stored, and deposited inside a syringe. However, this technology has several challenges and limitations. First, the printed object's resolution is typically low since it is often dictated by the extrusion nozzle diameter, which is a few millimeters.[4,5] Second, if the printing composition contains cells, they experience shear forces that may negatively affect their viability.[6] Third, a rapid fixation mechanism is required, often based on rheology or printing within a reactive liquid, thus limiting the printing compositions to a small range of polymers.

As opposed to DIW technologies, stereolithography-based 3D printing enables the fabrication of objects through light irradiation within a vat, which initiates localized photopolymerization reaction, resulting in micron-length scale down to submicron resolution.[7] Therefore, the ink should contain a photoinitiator (PI) and reactive monomers.[8]

In the Digital Light Processing (DLP) approach, a stereolithography-based approach (technology), 3D objects are constructed through layer-by-layer polymerization. Optimizing printing parameters, such as light intensity and duration, as well as controlling the printing head movement, is essential for obtaining high-quality 3D objects.[9]

Most bioinks used in DLP consist of one or a combination of two main components: Synthetic monomers with functional groups capable of undergoing polymerization, such as acrylamide or poly(ethylene glycol) diacrylate. The second is biopolymers with covalently bonded reactive groups, such as gelatin-methacrylate (GelMA). However, both approaches rely on synthetic components, which can adversely affect the bioink and the printed structures' biocompatibility and potentially hinder their suitability for biological applications.[10] So far, to the best of our knowledge, there is only a small number of publications on using non-functionalized biopolymers in DLP printing, for example, printing keratin with riboflavin as the PI, SPS as catalyst, and hydroquinone.[11]

The utilization of protein-only bioinks offers several significant advantages, including improved biocompatibility and overcoming the need for chemical modification of the biopolymer, such as methacrylate attachment on gelatin (e.g., GelMA).[7,12,13] In this research,

we used non-functionalized gelatin, an abundant protein derived directly from collagen, which plays a crucial role in forming the Extra-Cellular Matrix (ECM). It has been extensively utilized for numerous applications in the food industry [14] and in medical devices, including the formulation of drug delivery capsules and implants.[15] Given its wide range of applications and established safety profile, significant motivation exists to explore using gelatin as a biocompatible material for biological applications such as regenerative tissue engineering and wound healing.[16] Gelatin possesses many advantages, including good biocompatibility, solubility, degradability, easy acquisition, low price, and lower antigenicity compared to collagen.[17]

Moreover, gelatin keeps up the arginine-glycine-aspartic acid (RGD) peptide sequence, which favors cell adhesion, proliferation, and differentiation and, therefore, can play an essential role in fabricating efficient bio-scaffolds for medical implants.[18] Like other water-based printing compositions, there are noteworthy challenges in printing gelatin, including gelling at high concentrations and low temperatures and the necessity for water-soluble constituents only. Among them, water-soluble PIs pose a significant obstacle due to limited availability and low efficiency.[19,20] Non-modified gelatin contains the amino acid tyrosine, which can undergo a photopolymerization reaction to form di-tyrosine bonds that enable crosslinking of the protein in solution. Di-tyrosine bonds can be formed using a water-soluble PI, $[\mathrm{Ru(bpy)_3}]^{2+}$complex, and sodium persulfate (SPS) (the system is denoted as Ru/SPS).[21,22]

Photopolymerization is frequently initiated by ultraviolet (UV) or visible light; however, UV light may increase DNA mutations and instability of chromosomes, which further lead to apoptosis and affect cell viability. Thus, visible light is considered to be more biocompatible than UV light for bioprinting.[23] Ru/SPS enables crosslinking of native gelatin when irradiated with light within the visual spectrum (400 - 700 nm), having an absorbance peak at 450 nm.

Upon irradiation, the Ru(II) complex and persulfate composition undergoes photolysis, forming Ru(III) and sulfate radicals. The Ru(III) species functions as an oxidizing agent, facilitating the oxidation of tyrosine residues and generating tyrosine radical intermediates. These tyrosine intermediates then undergo arene coupling with neighboring tyrosine groups, a process further stabilized by the persulfate radicals and the removal of a hydrogen atom.[21] Lim et al. demonstrated that the utilization of Ru/SPS as a photo-oxidation system, in comparison to the conventional PI (Irgacure 2959, for example), offers distinct advantages. Specifically, the Ru/SPS system exhibits decreased oxygen inhibition and maintains superior cell viability, even under high concentrations and high light intensity. For instance, when the light intensity is

raised from 3 to 100 mW cm-2, the cell viability with Irgacure 2959 decreases from 90% to approximately 45%, whereas the Ru/SPS system maintains the cell viability at around 90%.[24] To the best of our knowledge, the utilization of pristine protein-only photopolymerization-based 3D printing has been documented in only a few publications, each employing a different technique. We previously reported successfully printing resilin protein using a two-photon printing approach,[25] which resulted in small-scale scaffolds, typically on the micron scale, under high-intensity irradiation. Xie et al. printed silk-based proteins only by Volumetric Additive Manufacturing (VAM), a compelling 3D printing technique still in its nascent stages of development.[26] Two additional reports on printing proteins only were introduced about keratin[11] and silk fibroin[27] printed in DLP using riboflavin as a PI, with very long irradiation times, 3-4 minutes per layer. Another recent relevant publication by Soliman et al. employed pristine gelatin in a bulk hydrogel as a delayed sacrificial ink, where gelatin and Ru/SPS formulations were irradiated in different 2D structures by a DLP printer, similarly to what can be achieved by soft lithography processes.[28]

As mentioned above, protein-based scaffolds printed by stereolithography processes can offer advantages over the commonly used materials. Biocompatible scaffolds are temporary templates that provide a suitable microenvironment for cells to adhere, proliferate, and differentiate, ultimately facilitating the regeneration of damaged or diseased tissues.[29,30] Cartilage tissue engineering has emerged as a promising approach to address the limited regenerative capacity of cartilage tissue.[31] Two main therapeutic strategies have been extensively explored: *in vivo* and *ex vivo*/*in vitro* cartilage tissue engineering. *In vivo* approaches involve implanting engineered cartilage constructs directly into the defect site within the living body, allowing the construct to benefit from the native environment and vascular supply, potentially promoting more biomimetic cartilage formation and integration with the surrounding tissue.[32,33] Conversely, *ex vivo* or *in vitro* approaches involve culturing and maturing the engineered cartilage construct in a controlled laboratory environment before implantation, enabling precise control over culture conditions and monitoring of construct properties.[34–36] Implementation of both approaches requires a biocompatible scaffold that will be populated by the cells and support their differentiation and maturation into mature tissue. Recent efforts, including ours, have focused on developing advanced scaffolds that can support and guide cartilage regeneration. Scaffolds with tailored architecture, mechanical properties, and bioactive cues are being investigated to provide a biomimetic environment for chondrocyte

growth, proliferation, and cartilage matrix production.[34–37] Additionally, the advent of 3D bioprinting technology has enabled the fabrication of highly precise and customized scaffolds, offering the potential for patient-specific implants and improved integration with native cartilage.[33,34,36–38] The above studies utilized either methacrylated proteins such as silk-glycidyl-methacrylate, GelMA, or synthetic polymers such as PCL.

This study presents novel DLP 3D printing compositions that utilize only non-modified gelatin to fabricate complex 3D structures for applications such as cartilage. The crosslinking mechanism relies on irradiation at visible light, which is not harmful to the cells. Both cell-seeding and cell-laden approaches were evaluated, and preliminary biological experiments indicate the potential of the gelatin scaffolds in making high-resolution cartilage implants.

2. Results

2.1. Ink formulation and optimization

Gelatin is considered a thermo-responsive material, as it undergoes a reversible sol-gel transition between solution (known as "sol" phase) and amorphous solid (known as "gel" phase). This process results in significant changes in the viscoelastic properties of the material, making it an important factor in view of printability and workability since the mobility of the reacting molecules is an essential factor for the polymerization process.[39] A series of gelatin solutions were prepared to test the printing process's suitability. The hydrogel exhibited poor shape fidelity below 10 wt.% gelatin, unable to maintain its original shape after polymerization. Conversely, formulations with gelatin concentrations exceeding 15 wt.% required high temperatures to be printed due to the high viscosity at room temperature. At a gelatin concentration of 30 wt.%, a printing temperature of around 60 °C was found to be optimal. Notably, the ink formulation also included SPS, which undergoes thermal activation above 70 °C for an extended duration,[40] and therefore, a practical upper limit of 30 wt.% gelatin was selected for the subsequent printing experiments.

The rheological properties of three gelatin solutions are presented in **Figure S1**, supplementary information). As expected, higher concentration led to higher viscosity. Interestingly, a hysteresis loop was observed during the measurements, which involved two measurement stages: heating from 10 °C to 60 °C, followed by a cooling stage back to 10 °C. Because of this hysteresis, the gelatin solutions were prepared at a high temperature, 65 °C, while the printing experiments were performed at 50 °C.

The printing experiments were performed according to the scheme presented in **Figure 1**. In essence, the protein solution contained the Ru/SPS initiator, placed in the heated DLP vat, and irradiated at 405 nm via a layer-by-layer process, according to the sliced CAD file. The resulting object is a crosslinked hydrogel rinsed off with water (80 °C) to remove all unreacted gelatin.

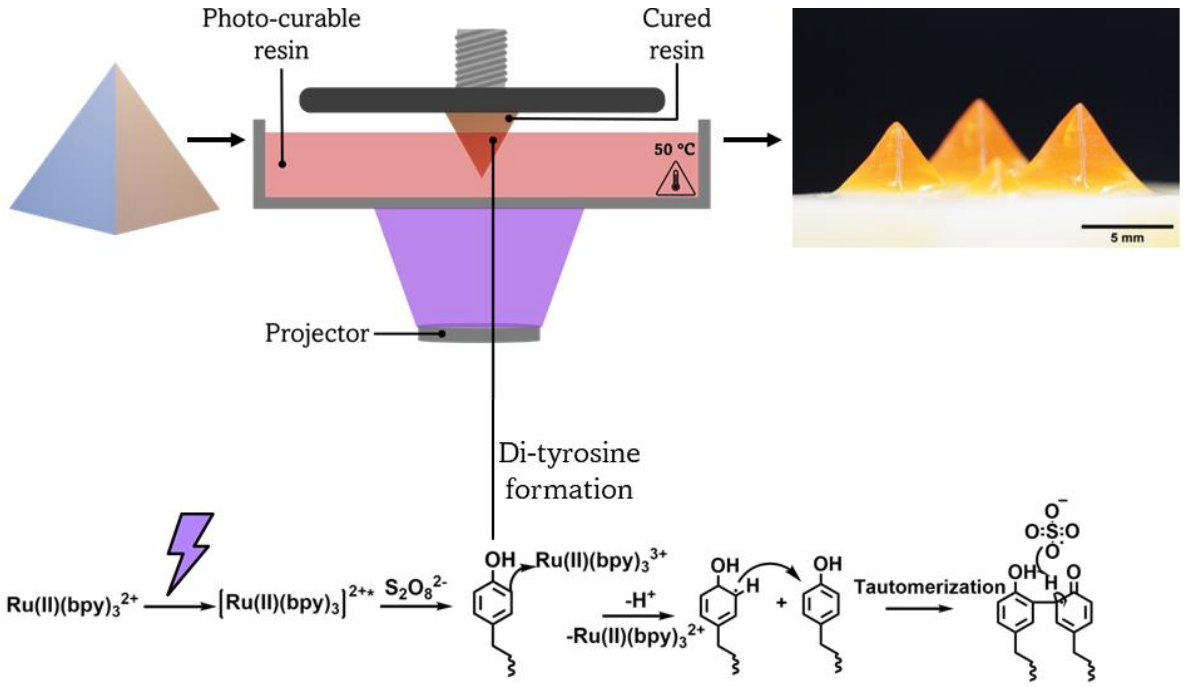

Figure 1. Schematic presentation of the DLP printing process for non-modified protein-only ink. The procedure commences with the design of a CAD file, subsequently fed into slicing software that translates the 3D CAD design into a sequence of 2D patterns. These patterns are projected onto the photocurable ink, directing the initiation of a photo-chemical di-tyrosine reaction at specific locations as dictated by the pattern.

2.2. Optimization of printing parameters

2.2.1. Cure depth evaluation

When fabricating each layer by the DLP process, the depth to which the light beam penetrates the resin critically governs each voxel dimension. As established by Jacobs, the cure depth can be expressed by the following relationship:[41]

$$\text{Equation 1: } Cd = D_p \cdot ln\left(\frac{E}{E_c}\right)$$

Where *Cd* – cure depth, *Dp* – penetration depth, *E* – energy dosage, *Ec* – critical energy. It is important to note that the energy dosage is the product of light intensity, given in units of mW cm^{-2}, and the exposure time in seconds.[42]

The cure depth of various formulations was evaluated by irradiation within the DLP vat at given energy doses and by measuring the thickness of the cured layer with an optical microscope (**Figure 2A**). **Figure 2B** shows the cure depth as a function of exposure time for two light intensities. As seen, increasing the exposure time led to increased thickness for both light intensities, leveling off at the higher intensity and long irradiation duration. As shown in **Figure 2C**, the cure depth of formulations without a dye and with Phenol red and Tartrazine were linearly dependent on the natural logarithm of the energy. According to Jacob's equation, the curve's slope represents the formulation's penetration depth, while the y-intercept corresponds to the critical energy required for polymerization. Interestingly, the critical energy for the composition without a dye was 28.8 mJ cm^{-2}, compared to 38.1 mJ cm^{-2} and 154.4 mJ cm-^{2} for compositions containing Tartrazine and Phenol red, respectively.

Subsequently, the cure depth was calculated for several theoretical light intensities, and the results are plotted as a function of exposure time (**Figure 2D**). This analysis enabled the identification of a specific light intensity that would allow easy tuning of the cure depth while maintaining short printing times. As seen in Figure 2D (inset), at high light intensities, the slopes are steep, thus predicting significant changes in cure depth upon minor changes in exposure time. Conversely, lower intensity levels require printing times that are too long. Therefore, we selected irradiation of 7.5 mW cm^{-2} for which the cure depth is not very sensitive to irradiation time, and yet it enables printing in short durations, ~40 seconds.

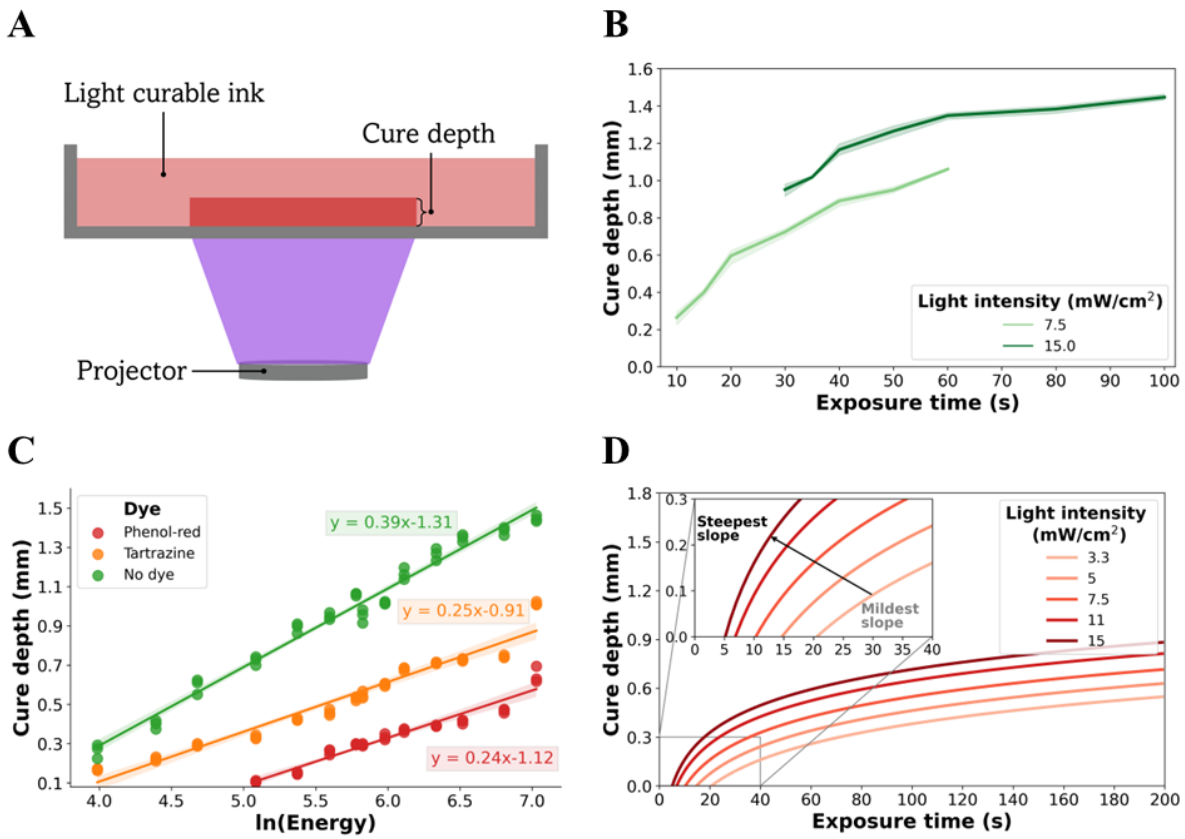

Figure 2. Cure depth analysis enables a deeper understanding and better customization of the printing parameters. (A) The experimental setup involves subjecting each ink formulation to light exposure and subsequently measuring the depth of the polymerized layer. (B) Cure depth measurements for ink formulation without dye for two light intensities (3 reps). (C) Linear trends were observed for each formulation's cure depth, which correlates with the natural logarithm of the energy (N=3). (D) Calculated cure depth was determined for a range of light intensities as a function of exposure time. All error bars represent confidence intervals.

2.2.2. Resolution improvement by photo-absorbers

Confining the polymerization area to small spots is crucial to achieve a high dimensions similarity between the CAD file and the printed object. This can be accomplished by employing photo absorbers (dyes) that can absorb a certain amount of light without causing polymerization. For bioprinting applications, selecting appropriate dyes becomes crucial, as they should absorb the specific wavelength and yet be non-harmful to living systems.

Phenol red emerges as a promising candidate for the intended application due to its absorption characteristics around 400 nm and its frequent use in cell culture media. It has a very low toxicity, excellent stability within living systems, and minimal interference with biological processes [43]. Tartrazine, another pertinent dye, has been employed in diverse cell-related systems, serving as a coloring agent in food and cosmetic products [44]. **Figure 3A** shows that

formulations containing these dyes exhibit stronger absorbance at the relevant wavelength of the printer (405 nm), making them suitable choices for investigation as potential resolution enhancers in the ink formulation. The UV-Vis spectra of the various solutions are presented in **Figure S2**, along with the printer's irradiation peak and intensity. As described above, the critical energy of polymerization was the highest for Phenol red, 154.4 J cm^{-2}. Thus, it should be very effective in controlling resolution, and therefore, the subsequent experiments were performed with this dye.

The XY resolution was evaluated by printing rectangles and comparing their dimensions to the corresponding CAD file. This assessment involved measuring the area of each printed rectangle using ImageJ software. **Figure 3** shows the % area printed/theoretical area for each formulation at various exposure times, while 100% is defined as the highest resolution. Above 100% is termed overcuring, and below 100% is termed under-curing. In general, as expected, the higher the exposure time, the larger the printed area compared to the designed area. The formulations without dye and with Tartrazine were always overcured (and at lower exposure time, did not cure at all).

In comparison, the formulation containing Phenol red was either over-cured or under-cured, while at 40 seconds exposure, the ratio was 100%, meaning excellent resolution. Therefore, the subsequent printing experiments were performed at the same irradiation energy (300 mJ cm^{-2}). These experiments were under irradiation intensity, meaning that in view of energy, the irradiation time can be shortened by increasing the intensity.

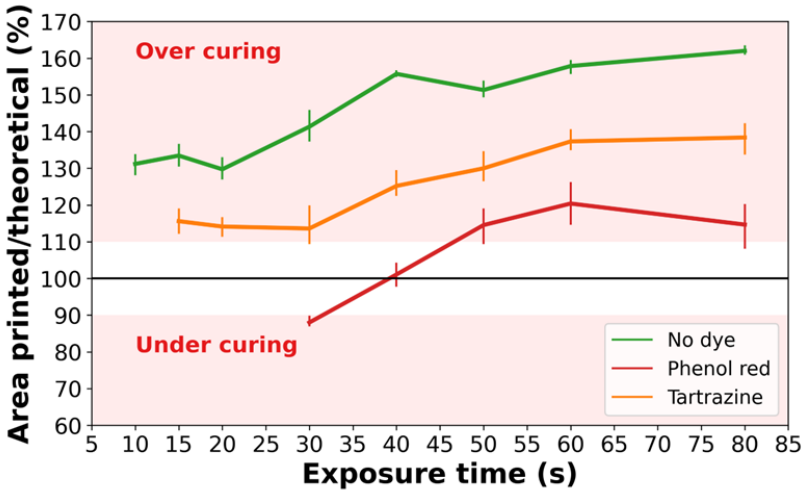

Figure 3. Addition of dye improves XY-resolution. Area printed/theoretical (%) for each formulation at various exposure times were evaluated for each formulation (without dye, with Tartrazine, and with Phenol red). 100% resemblance is shown as a black line. Error bars represent confidence intervals.

2.3. 3D Printed models

By using a gelatin concentration of 30 wt.%, simple shapes could be 3D printed, e.g., pyramids shown in Figure 1. However, for more complex structures, it was found that it was necessary to decrease the gelatin concentration. After evaluating various concentrations, a 22.5 wt.% was selected, enabling printing structures as shown in **Figure 4**. Interestingly, the printed hydrogel structures were stretchable, as seen in Figure 4B and videos S1 and S2 in the supplementary information. Another noteworthy feature of the printed gelatin structures is their response to pH change, in view of swelling and color, which makes the object classified as 4D printed. The printed structures were immersed in aqueous solutions having various pH values. As seen in Figure 4A, the objects swell with the increase in pH, with higher pH values leading to more substantial swelling. The swelling increases by ~140% while immersed at pH 12 compared to pH 4. This phenomenon results from the deprotonation of the gelatin (type B, isoelectric point of 4.5),[45] as the gelatin molecules are crosslinked.

The use of Phenol red as a dye also enables color and response while the pH is the stimuli, as shown for other 4D printed objects.[46,47] At pH 4, the hydrogel containing Phenol red displayed a yellow color, and as the pH increased, the hydrogel transitioned to a solid red appearance at pH 12. This pH-dependent color shift further highlights the potential use of colorants, including PR, in bioprinting applications at which pH monitoring or visual detection is essential, such as wound healing applications.[48,49]

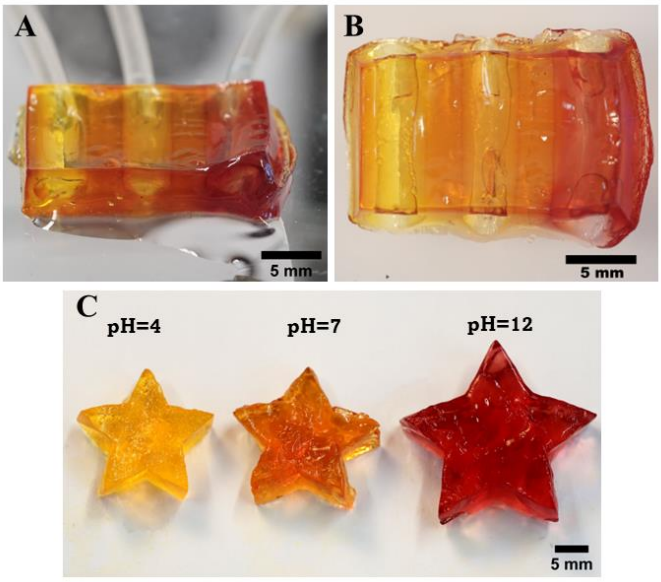

Figure 4. 3D printed models based on non-modified gelatin only. (A) Phenol red has the unique property of pH-dependent color change, (B) stretchable network-shaped printed hydrogel, and (C) examples of various printable shapes and sizes.

Once the optimal composition and printing parameters are defined, printing hydrogel structures with high complexity is realized. As presented in **Figure 5**, these printing compositions enabled the fabrication of overhanging structures and objects with embedded, open tubings, which are essential for bioprinting implants with blood vessels.

It's noteworthy that the majority of existing research in DLP printed hydrogels commonly uses proteins with covalently bonded polymerizable groups or compositions, including synthetic monomers. Conversely, prior published works employing protein-only formulations typically encompass much lower protein concentrations than our current research, a feature that can significantly impact biocompatibility aspects. Figure 5G presents the published work with DLP printing of proteins, showing that there are only a few non-modified ones, while we use the highest reported concentration of non-modified protein.

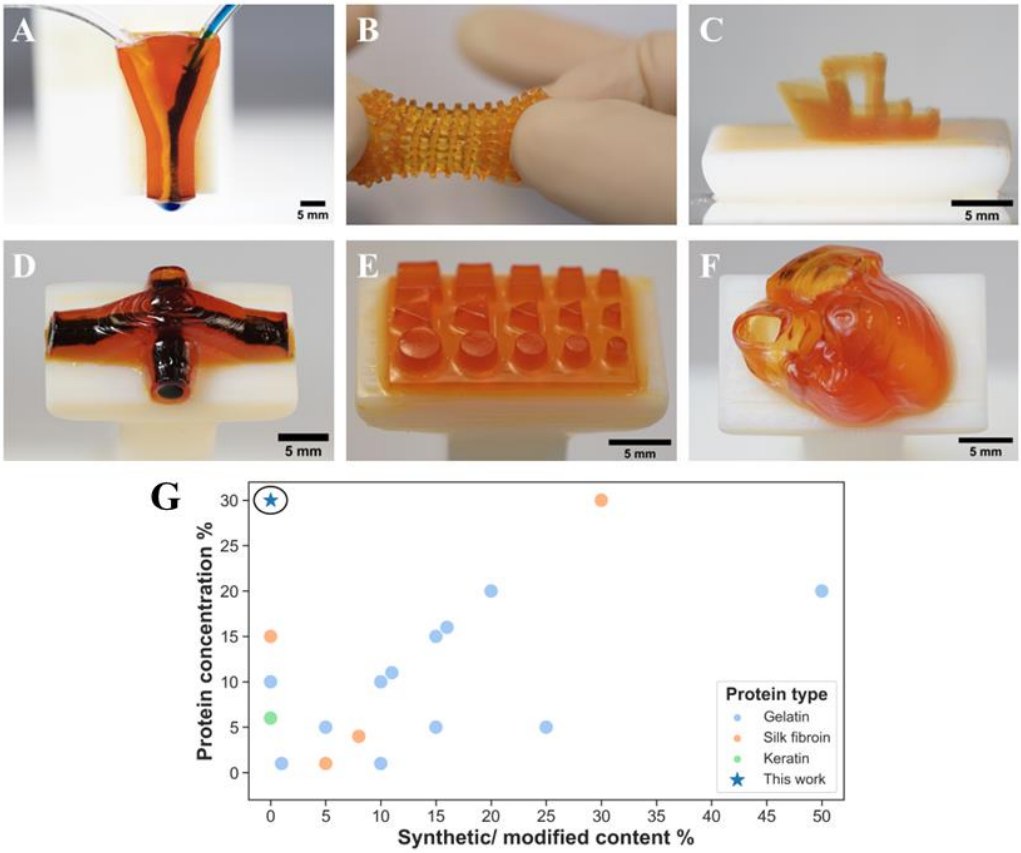

Figure 5. The suggested formulation utilizes only unmodified gelatin, allowing for relatively high protein concentration DLP printing of objects with different complexities. (A) Y-shaped pipes with two different colorant solutions, (B) stretchable woodpile, (C) Benchy, a boat shape demonstrating overhang, (D) Object with two internal open tubes, one above the other, (E) different geometrical objects, (F) Anatomical heart model, (G) Published works about DLP printing of proteins.

2.4. Mechanical properties of printed structures

To fabricate a functional and biocompatible 3D printed hydrogel, it is essential to tailor the material's mechanical properties to suit the specific application. The mechanical characterization of the printed structures followed two main paths. Initially, the focus was on how the hydrogel behaves under unconfined compression. Eight printed discs underwent a compressibility test, revealing a compression modulus of 31 kPa (**Figure 6A**). The printed objects have a modulus similar to soft tissues found in organs such as the liver, pancreas, and capillaries.[50] As a result, it is a suitable candidate for implantation and other bio-devices with similar moduli. The second approach involved oscillatory measurements, including amplitude and frequency sweeps. The storage and loss moduli from the linear viscoelastic region are presented in **Figure 6B** and **Figure S3** for measurements performed for five printed discs in each test.

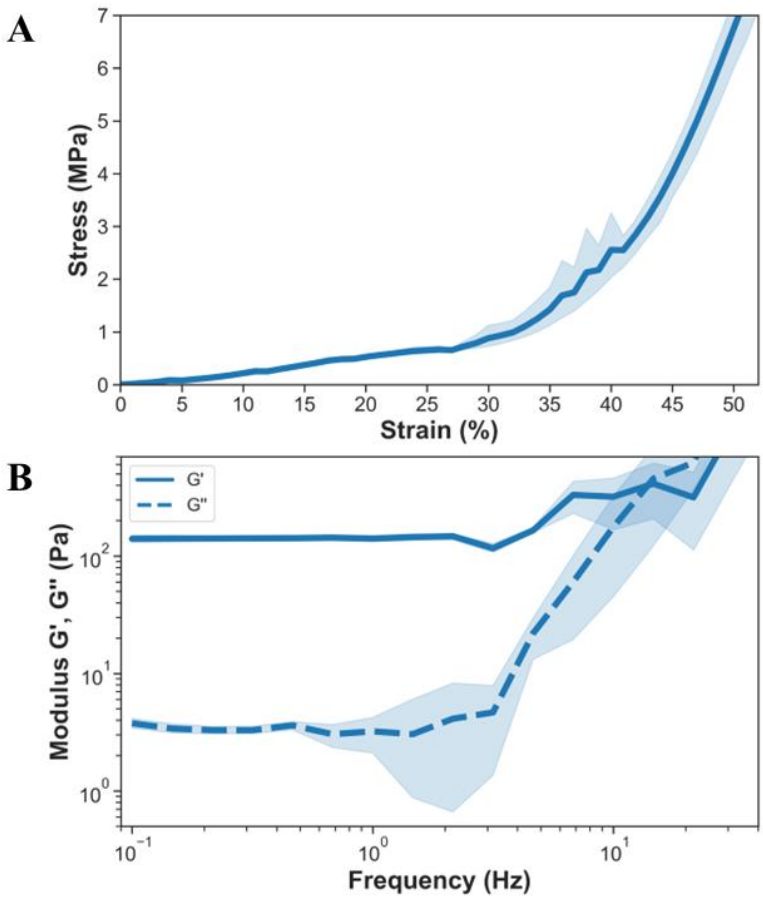

Figure 6. Mechanical properties examination. (A) stress-strain curve for printed discs (8 reps); (B) oscillatory frequency sweep (OFS) results for printed discs (5 reps). Both storage and loss modulus remained constant for frequencies between 0.1-2 Hz. Error bars represent confidence intervals.

2.5. Drying of printed objects

In electron microscopy characterization and some applications, the hydrogels must be converted to a solid while keeping their original shape and structural integrity without any cracks or other physical defects. When drying 3D printed hydrogels, avoiding shape retention and collapse of the desired object poses several challenges.[51] We have evaluated several drying methods that are commonly used in hydrogels: Simple drying at ambient or elevated temperatures, supercritical drying (SCD), and lyophilization.

It was found that utilization of SCD for crosslinked gelatin-based hydrogels was not feasible due to the process prerequisite of solvent exchange into ethanol, isopropanol, or methanol. Any immersion of the printed objects into these solvents led to the immediate collapse of the gel structure (Figure S2, supporting information). Even with a gradual solvent exchange, large flakes were formed when the solution concentration exceeded 40% for all tested solvents.

Following this unsuccessful approach, an experiment was conducted to assess alternatives for the drying process of objects placed in soaking solutions by simple evaporation and lyophilization.

After several preliminary experiments, the three chosen soaking solutions were PBS, bovine serum albumin (BSA), and trehalose. The selection of PBS served as a negative control since it replicates the primary component within the printed object. BSA and trehalose were selected as potential lypho-protectants.[52,53]

The experiments were performed as follows. Six cubes were immersed in solutions, namely PBS solution (cubes 1 and 2), BSA (cubes 3 and 4), and trehalose (cubes 5 and 6), for 24 hours (**Figure S5**). Subsequently, the cubes were dried using either freeze-drying (cubes 1, 3, and 5) or allowed to dry at ambient conditions inside a fume hood (cubes 2, 4, and 6). Optical imaging and SEM cross-sectional imaging revealed that Cubes 1 and 3 have a porous structure and puffy appearance. Cube 5 exhibited a cracked structure without noticeable porosity. Conversely, cubes 2, 4, and 6 exhibited poor shape retention, displaying smooth surfaces (Figure S5). In conclusion, it appears that lyophilization after soaking in PBS and BSA results in porous structures that retain their original dimensions. It should be noted that the lyophilized sample can recover its initial shape with a somewhat distorted shape after re-immersion in a PBS solution.

2.6. Biological studies

Cell adhesion and growth onto and within the gelatin-based 3D constructs were evaluated by examining two cell fabrication techniques: (1) Cell-seeding onto the woodpile printed gelatin

scaffold and (2) printing compositions that contains living cells during the printing process (cell-laden). In the first approach the cells are not exposed to the light irradiation and the cell growth occurs upon attachment on the woodpile bars of the scaffold and continues to the voids. In the second approach the cells are exposed to light irradiation and are embedded within the gelatin matrix as the printing proceeds. Therefore, the cell growth in this case occurs within the polymeric network and continues to the voids between the woodpile bars. Cell survival may be impacted by both deficient adhesion conditions and irradiation, however we use light within the visible spectrum which should not be harmful to the cells.

2.6.1. Cell-seeding approach

By this approach it was found that chondrocytes seeded onto the 3D printed gelatin scaffolds showed adhesion, survival, and proliferation over 7 days of immersion in culture media.

Cultured human nasal chondrocytes were suspended in 8% gelatin to enhance initial adhesion and then applied onto the printed scaffolds, followed by incubation in growth media. Bright-field imaging demonstrated chondrocyte adhesion to the scaffold surface as shown in **Figure 7A**. Cell viability assay revealed viable cells at days 5 and 7 post-seeding as presented in **Figure 7B**. H&E histological analysis and Ki67 immunostaining confirmed the presence of proliferating chondrocytes which are distributed throughout the scaffold after 7 days (**Figure 7C** and **Figure 7D**). These results indicate that the 3D printed gelatin scaffolds support chondrocyte attachment and growth when seeded post-printing.

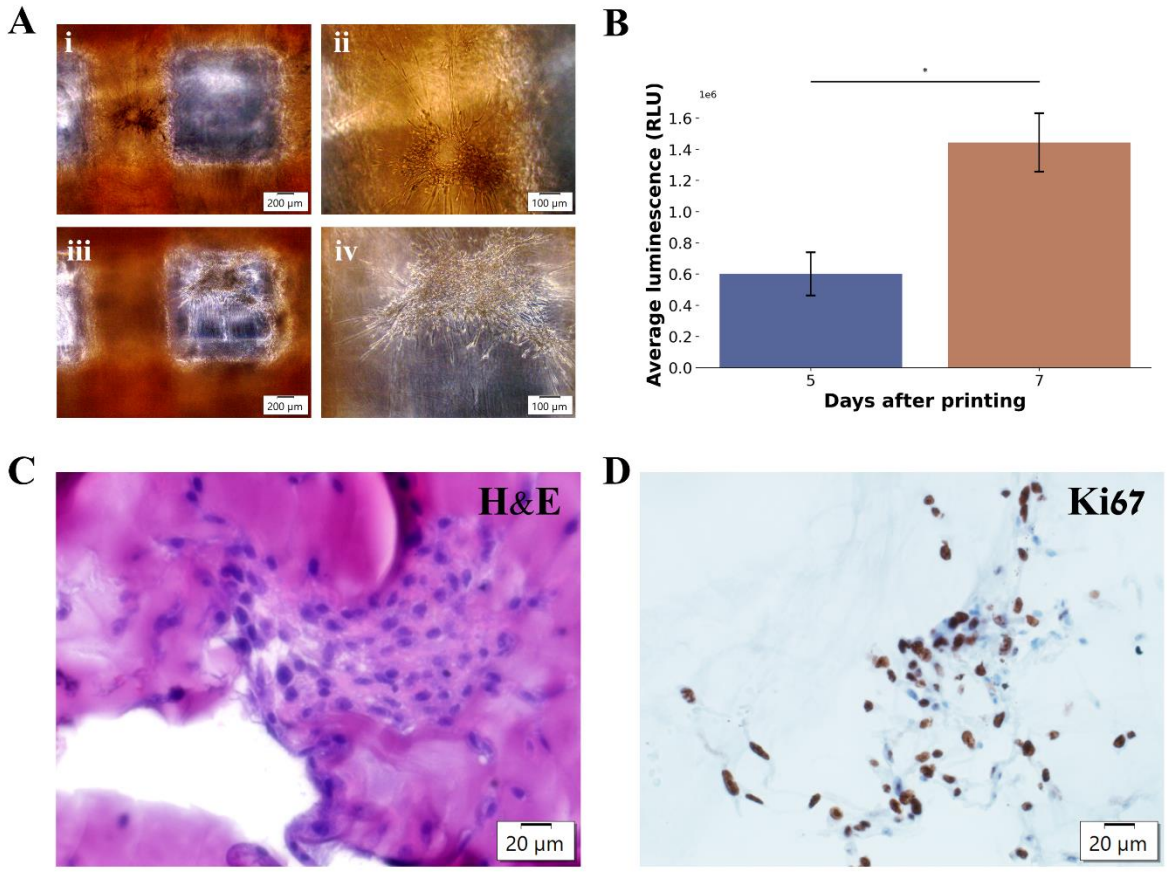

Figure 7. Chondrocyte viability and growth within 3D printed cell-seeding constructs. Chondrocytes were seeded onto the 3D printed scaffolds in a gelatin solution and grown for up to 7 days in cell culture media. (A) Bright-field microscopy images show cell attachment both on the surface (i, ii) and within the interior voids (iii, iv). (B) Cell viability assay demonstrates cell survival 5 and 7 days following chondrocytes seeding onto the printed scaffold, N=1, triplicate. H&E (C) and Ki67 (D) histological staining demonstrate cell adhesion, survival, proliferation, and distribution on the scaffolds after 7 days. Error bars represent standard deviation.

2.6.2. Cell-laden approach

In this part of the research, the cells were dispersed within the printing formulation, followed by a 3D printing process in which the cells were exposed to light irradiation and the mechanical forces occurring during printing. In general, it was found that chondrocytes remained viable, and the cell growth continued within the printing composition and after the printing process. Microscopy imaging showed the presence of embedded chondrocytes within the cell-laden constructs 4 days after printing (**Figure 8A** and **Figure 8B**). To evaluate the effect of the duration of the printing process on cell survival and proliferation, the printing was performed for 12 or 18 minutes, and the cells were subsequently cultured for viability analysis. The cell viability assay was performed at 24, 48, 72, and 96 hours and no significant

difference in viability was observed between the two printing durations, indicating similar proliferation capacity of the two groups (**Figure 8C** and **Figure 8E**). Trypan blue staining at day 7 further confirmed that cell viability and proliferation were maintained after the printing process (**Figure 8D** and **Figure 8F**).

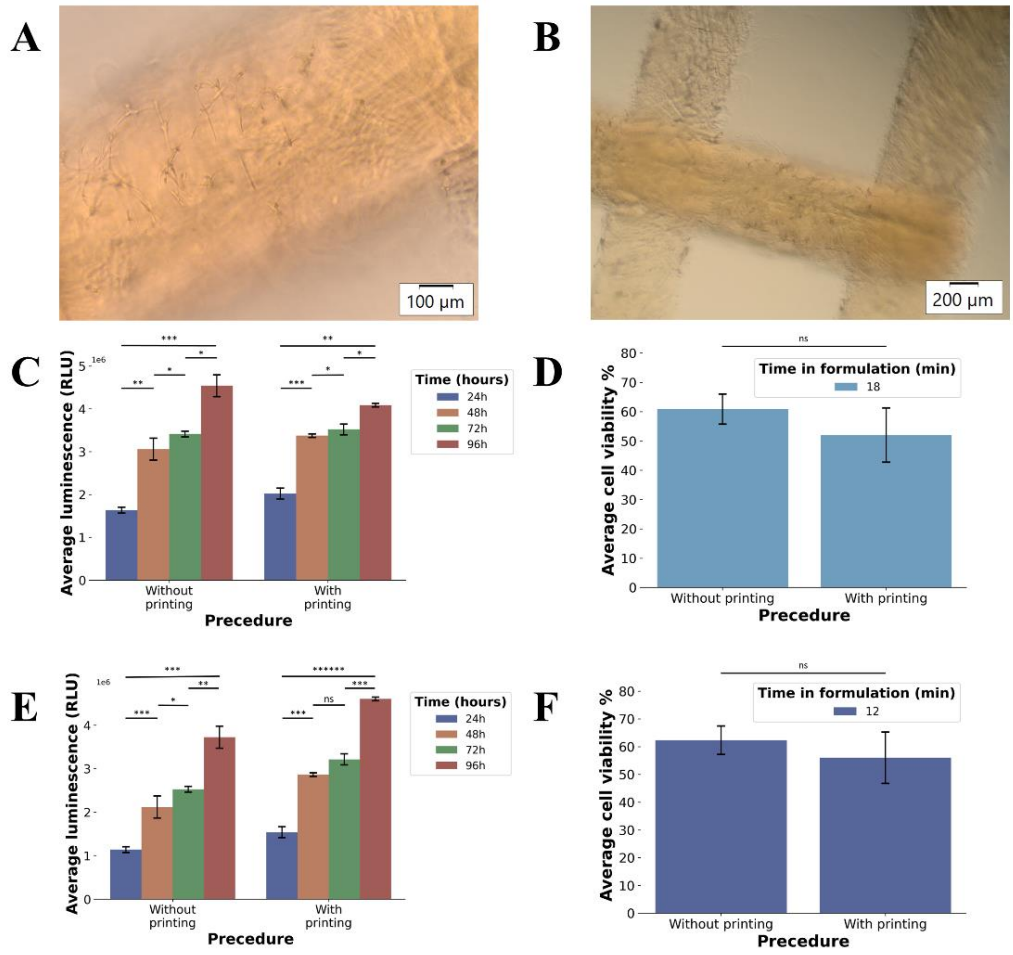

Figure 8. Chondrocyte viability and growth within 3D printed cell-laden constructs. Chondrocytes were encapsulated within the bioink formulation, 3D printed and grown for up to 7 days in cell culture media. (A, B) Bright-field microscopy images show viable, embedded chondrocytes within the constructs. (C) Cell viability assay demonstrates the chondrocyte viability and proliferation of cells that undergo 18 minutes print time at 24, 48, 72, and 96-hours post-printing. (E) Same as (C) for 12 minutes printing. (D, F) Cell counting using Trypan blue staining further confirmed the maintenance of chondrocyte viability and proliferation post-printing. For all tests shown N=1, triplicate. All Error bars represent standard deviation.

Overall, the findings in the preliminary experiments potentially establish that both the cell-seeding and cell-laden strategies enable successful 3D culture of chondrocytes within the gelatin-based constructs fabricated by the presented 3D printing of non-modified gelatin-only approach.

3. Conclusion

In this work, a pristine gelatin solution was photopolymerized by a rarely used Ru/SPS to fabricate complex objects using DLP. Ru/SPS transforms the linear chain of the gelatin to a crosslinked network by generating di-tyrosine bonds between the residues of two tyrosine amino acids. Therefore, we rely on the functional groups within the native protein; thus, the bioink is low-cost, as no chemical modification is required. This also decreases the risk of antigenicity responses for future biological applications. Additionally, we harness a new functionality of the dye Phenol red, which is used in cell culture media. Phenol red acts as a visual pH indicator of cell media and enables the detection of changes in pH and the taking of appropriate actions to maintain optimal conditions for cell growth and viability. Here, we use Phenol red as a photo-absorber to improve the DLP printing resolution and accomplish a biocompatible 3D printed object with an inherent pH visual indicator.

We demonstrated that complex 3D objects could be achieved using a typical DLP printer, reaching a high protein content of 30 wt.% gelatin. Thus, structures with different architectural complexities were successfully printed, showing the ability to print overhangs, open tubes and detailed features. Unlike traditional DIW methods used in bioprinting, which often suffer from low resolution and cell viability issues, this study presents the use of non-modified gelatin as a photocurable ink, relying on a di-tyrosine crosslinking mechanism, without a chemical modification or added monomers.

The printed object showed a compressive modulus of 31 kPa, which is in the region of soft tissues, relevant for the potential implantation use of the gelatin-based printed objects. Moreover, this study found that using PBS and BSA soaking solutions in lyophilization post-processing optimally preserved the shape of hydrogels during the drying process.

The biological results shown in the current study demonstrate the feasibility of using visible light-based 3D printing approaches to fabricate gelatin constructs for tissue engineering applications, specifically for engineering cartilage tissue. The results indicate that the 3D printed gelatin scaffolds support chondrocyte adhesion, survival, and proliferation, as evidenced by the cell-seeding experiments. Furthermore, the cell-laden printing approach, in which chondrocytes were incorporated directly within the gelatin formulation prior to printing, also enable maintaining cell viability and proliferative capacity for the tested durations.

These preliminary findings highlight the potential of this approach for medical applications involving the production of living tissue implants. However, further investigations are necessary to optimize the methods and protocols for specific tissue engineering applications.

Future studies will focus on identifying the specific conditions that promote optimal cell-seeding and distribution within the scaffolds, as well as conditions that encourage long-term cell survival, differentiation, and extracellular matrix secretion, ultimately leading to the maturation of functional cartilage tissue.

Overall, the formulation and printing process presented herein have the potential to revolutionize the use of non-modified protein-only bioinks for the fabrication of intricate 3D objects. This development is anticipated to open up new research avenues in biomedical engineering, making it possible to create previously unattainable structures with high fidelity and precision, while using pristine proteins.

4. Experimental Section

Materials: Gelatin from porcine skin – type B, $[Ru(bpy)_3]^{+2}$, Tartrazine, and sodium phosphate (dibasic and monobasic) were purchased from Sigma Aldrich. Sodium persulfate (SPS) was purchased from Holland Moran, Israel. Phenol red was purchased from Acros Organics.

Bioink preparation: Phosphate buffer saline (PBS) was prepared according to standard protocol [28]. Gelatin (30 or 22.5 wt.%) was dissolved in PBS and heated to 50 °C while stirring. Concentrated solutions of 40 mM $[Ru(bpy)_3]^{+2}$ and 400 mM SPS were diluted to a final concentration of 0.8 and 8 mM, respectively.

Fabrication of 3D structures in Mold: UV-curable solution was poured into a mold and irradiated for 60 sec with a 405 nm UV torch (32 DC V, 8 A).

DLP printing: predesigned CAD printed model was generated using a DLP printer (Asiga Max X35, Australia) equipped with a 405 nm LED. The printer's XY-axis resolution is 35 µm, while the maximum resolution on the Z-axis is down to 1 µm. The printing composition was poured into the designated heating bath heated to 50 °C. Each printed layer was 100 µm thick and was cured for 35 sec with a light intensity of 7.5 mW cm^{-2}.

The 3D objects STL files were obtained from Thingiverse, Anatomical heart by airforce (https://www.thingiverse.com/thing:942464, license: CC-BY-SA), 3D Benchy by Creative-Tools (https://www.thingiverse.com/thing:5293974, license: CC-BY-ND). All other STL files were designed with Autodesk Inventor software.

Electron microscopy: Scanning Electron Microscope (XHR-SEM) images were obtained using an extra-high-resolution scanning electron microscope (XHR Magellan 400 L).

UV-Vis spectrophotometry: UV-Vis spectrophotometry was used to quantify the ink components' absorption. Spectrophotometric measurements were recorded using a UV-spectrophotometer (UV-1800; Shimadzu, Japan). Absorption spectra of ink components (gelatin, gelatin with PI, and gelatin with PI and various dyes) were recorded in the spectral range of 300 to 800 nm with a resolution of 0.5 nm.

Compression test: to perform the compression test, discs (10 mm in diameter and 5 mm thick) were printed using bioinks and washed with hot water for 5 min.

Compression mechanical tests of the obtained discs were performed on the fully cured samples using an Instron universal testing machine (Model 3345, Instron Corp., Norwood, MA) equipped with a 500 N load cell. The compression test was conducted at 25 °C using 10 mm min-1 crosshead speed.

Dynamic Mechanical Analysis: discs with a nominal sample size of 10 x 5 mm (diameter x height) were printed to evaluate DMA properties. Rheometer (RheoStress HAAKE 6000) was used with a parallel plate geometry (P35 Ti L – 60 mm) at 25 °C. Oscillation Amplitude Sweep (OAS) was carried at a frequency of 1 Hz, and a range of shear stresses of 0.1-1,000 Pa was tested. The gap between the plates was set to fit 1.5 N.

After identifying the Linear Viscoelastic Region (LVER) from the OAS tests, the desired shear stress (Tau) for later assays was chosen. Oscillation Frequency Sweep (OFS) was carried at shear stress of 1 Pa for frequencies of 0.1-100 Hz. The gap between the plates was set to fit 1.5 N.

Cell isolation and expansion: Tissue sample collection was approved by the Sheba Medical Center Ethics Committee (4745–17-SMC). All patients signed consent forms. Chondrocytes were isolated from nasal cartilage as previously described by our group.[34] In brief, nasal cartilage was cut into 1-3 mm pieces, incubated with collagenase II for 12-14 hours, and washed with growth medium (DMEM/F12 with 10% fetal bovine serum, and 1% pen-strep) following a 100 µm strainer filtration. After being centrifuged at 600 x g for 8 minutes, the cells were cultured with growth medium replacement every 2-3 days until reaching a confluence of 80%.

Chondrocyte seeding onto printed gelatin scaffolds: Chondrocytes at passage two were trypsinized (0.25% trypsin - biowest) and washed with growth medium. Following cell count, the supernatant was gently aspirated, and the pellet was suspended (30 µL of 8% gelatin at 37°C) and seeded drop-wise onto the gelatin scaffolds at a cell concentration of 15-30x104/µL.

The seeded scaffolds were incubated at 37 °C in a humidified atmosphere of 5% CO2 in air in a growth medium and replaced every 2-3 days.

Viability Assays: Cell viability was assessed using two methods: cell counting and a luminescence-based assay. samples were collected from the gelatin formulation before and after printing. Chondrocytes were seeded in triplicate at a density of 3,000 cells/well in 96-well plates following four consecutive washes with PBS at 37°C. For cell counting, cells were stained with Trypan Blue (Biological Industries) at a 1:1 ratio, and viable cells were counted using a CellDrop BF Bright Field cell counter (DeNovix). For the luminescence assay, cell viability was evaluated using the RealTime-Glo™ MT Cell Viability Assay (Promega) according to the manufacturer's instructions. Luminescence was measured using a GloMax plate reader (Promega).

Histology and Immunostaining: After 7 days of culture, cell-seeded scaffolds were fixed (4% formaldehyde) for 24 hours and embedded in paraffin at 65°C. The scaffolds were sectioned at 5 µm thickness, deparaffinized with OmniPrep solution (ZytoMed) for 40 minutes at 80°C, rehydrated, and stained with hematoxylin and eosin (H&E) for morphological analysis. For immunostaining, sections were permeabilized, washed with PBS, and blocked with BSA solution for 1 hour. Sections were then incubated with a Ki67 primary rabbit monoclonal antibody (1:300, ePredia by Fisher Scientific) according to the manufacturer's instructions, mounted, and imaged using a light inverted microscope (Olympus IX83, Olympus, Japan).

Statistical Analysis: Statistical analysis was performed using a two-tailed unpaired Student's t-test. Differences between groups were considered statistically significant when the p-value was ≤ 0.05. P-values symbols legend:

>0.05	ns
≤0.05	*
≤0.001	**
≤0.0001	***
≤0.00001	****
≤0.000001	*****
≤0.0000001	******

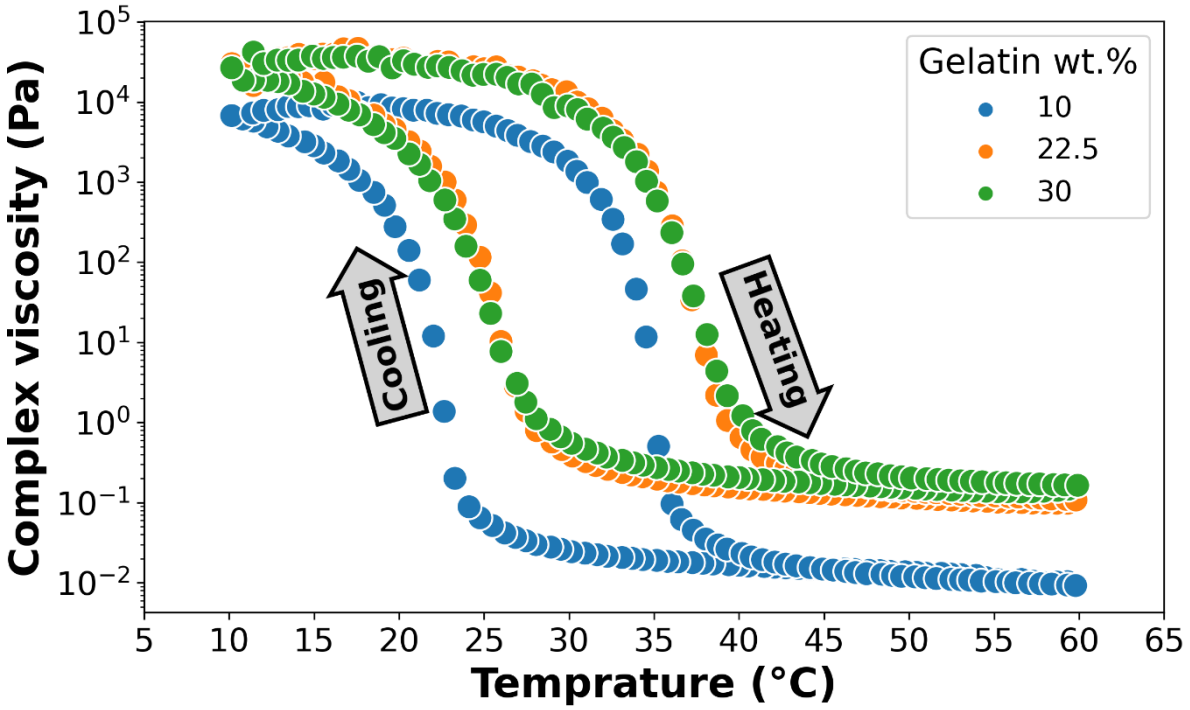

Figure S1. Temperature history dictates different gelation points between the cooling and heating stages, emphasizing the use of the lower gelation point to achieve the ink viscosity requirement for DLP bioprinting. Temperature ramp test for gelatin type B at various wt% resulted in a hysteresis loop. The lower gelation point was measured for the cooling stage compared to the heating stage.

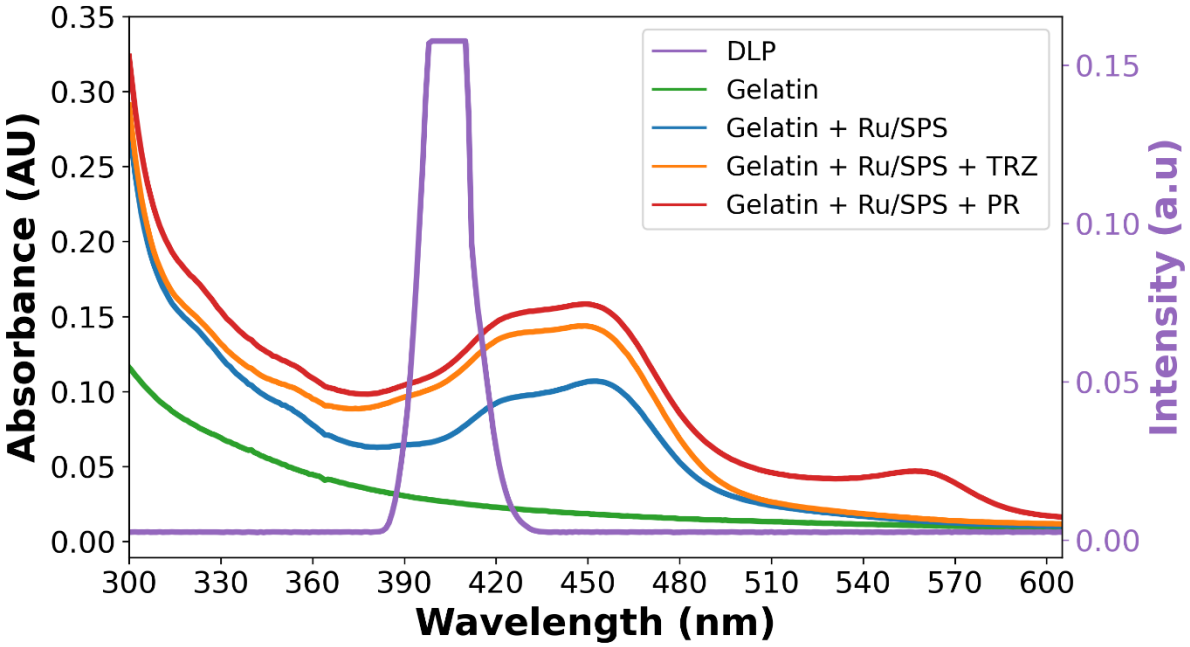

Figure S2. Absorbance of several formulations, different in photo-absorbers components. Including gelatin solution (green), gelatin with Ru/SPS (blue), gelatin with Ru/SPS and Tartrazine (TRZ) as a dye (orange), and gelatin with Ru/SPS and Phenol red (PR) as a dye (red). Irradiation intensity of DLP printer in the relevant wavelengths.

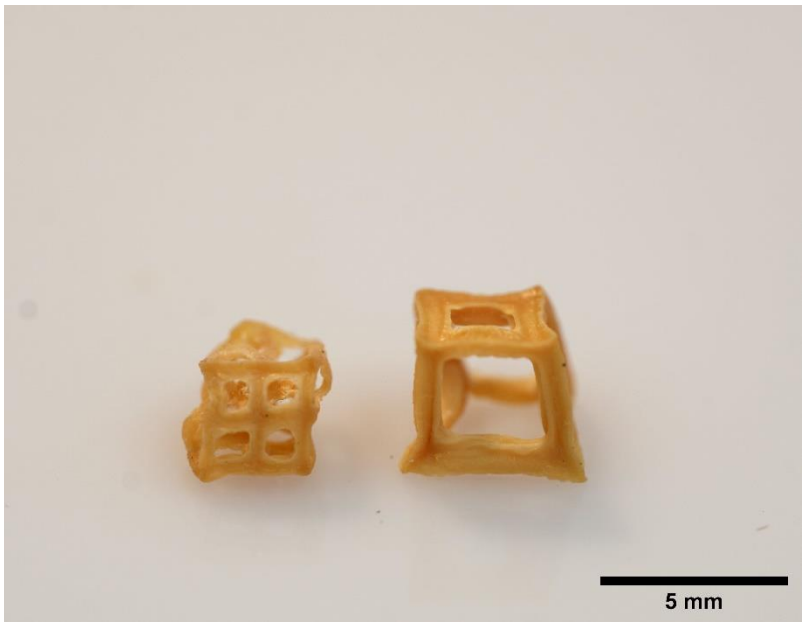

Figure S3. Gelatin-only hydrogel immersed in isopropanol leading to shape distortion.

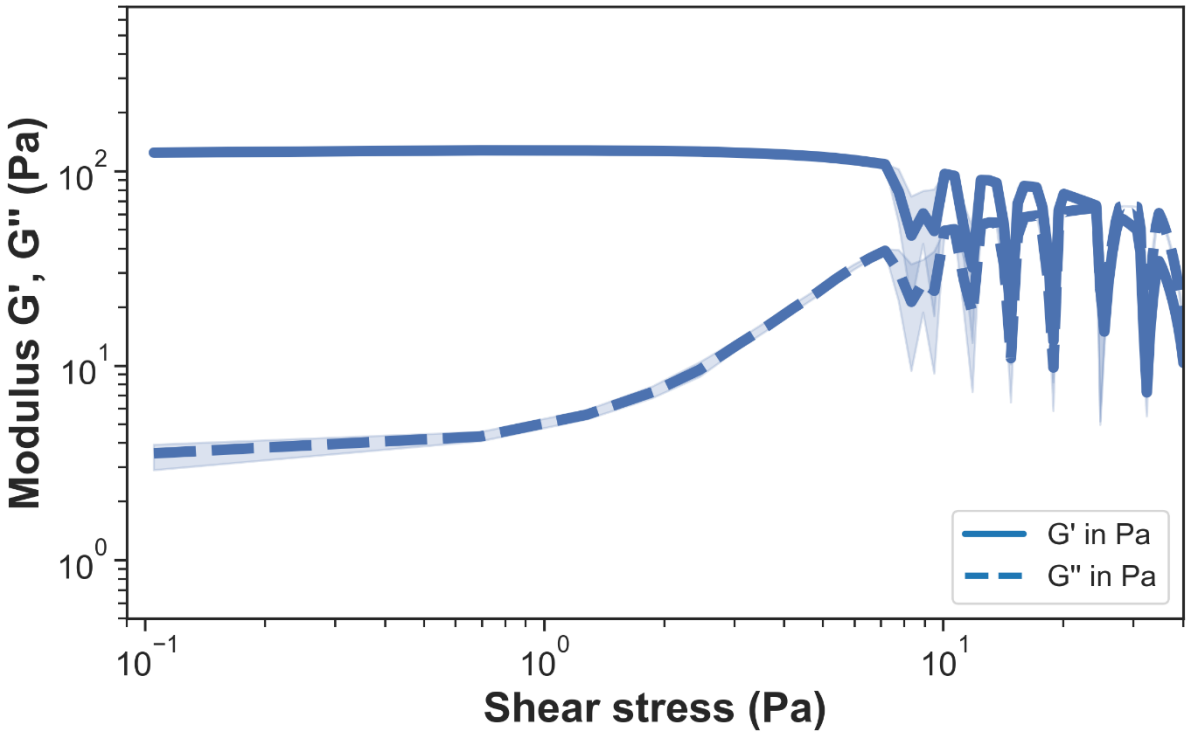

Figure S4. Oscillation Amplitude Sweep (OAS) results for printed discs (N=5). Based on these results, the LVER was identified, and a shear stress of 1 Pa was selected for OFS tests.

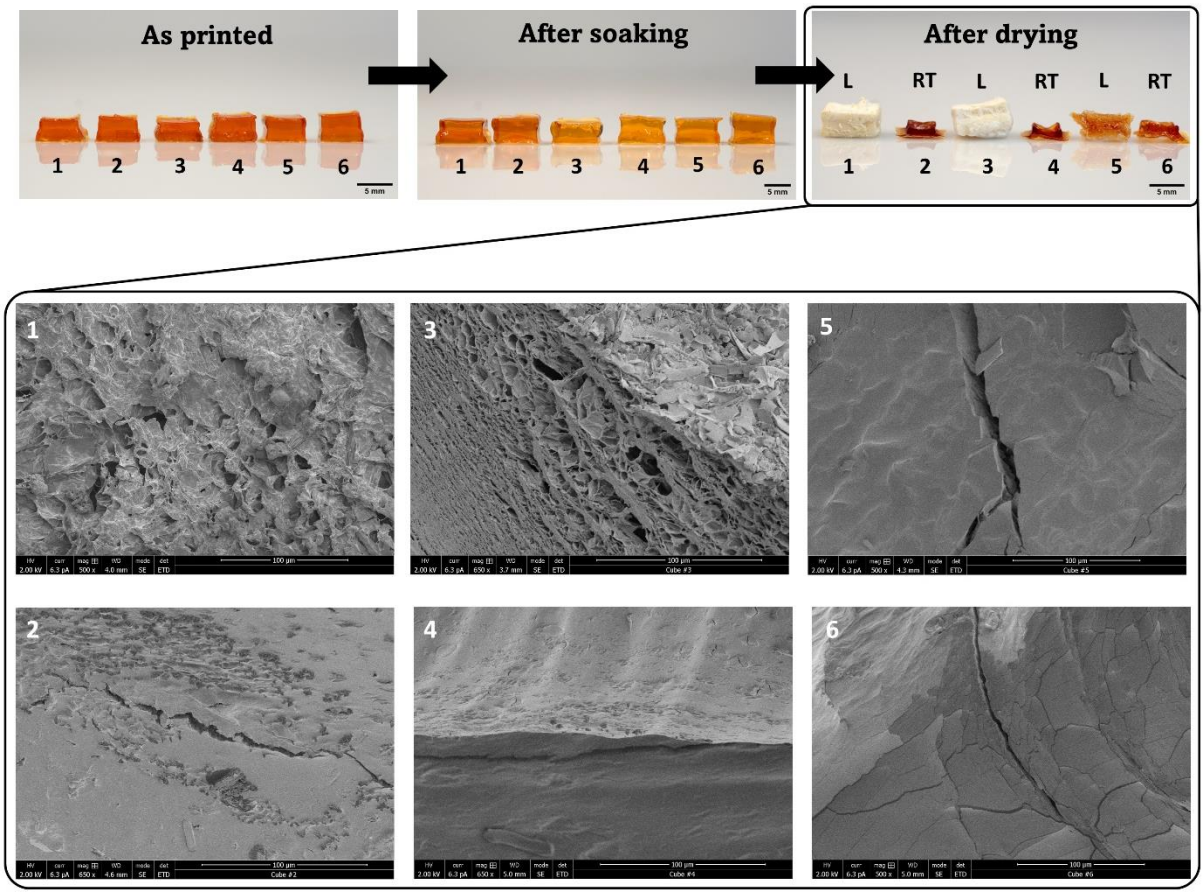

Figure S5. Different drying methods result in different porosity and shape retention. Six cubes demonstrate six drying options, each soaked for 24 hours and dried in ambient conditions or freeze-drying. L- Lyophilized, RT–dried in ambient conditions (room temperature).

Acknowledgements

Ayelet Bunin thanks to the HUJI nano center M.Sc. program in Chemistry with specialization in Nanoscience and Nanotechnology.

Funding: This work was supported by the Israel Innovation Authority grants numbers 81144 and 81145.

Author contributions: Conceptualization: D.K., O.H.S, S.D., and S.M. Investigation: A.B. L.L, M.F.G., T.K, B.S. Supervision: O.H.S, S.D., and S.M. Writing—original draft: A.B. Writing—review & editing: A.B, D.K., O.H.S, S.D., and S.M.

Conflict of interests: The authors declare no conflict of interest.

References

[1] A. Al-Abboodi, S. Zhang, M. Al-Saady, J. W. Ong, P. P. Y. Chan, J. Fu, *Biomedical Materials* **2019**, *14*, 045010.

[2] A. J. R. Amaral, V. M. Gaspar, P. Lavrador, J. F. Mano, *Biofabrication* **2021**, *13*.

[3] B. Frost, B. P. Sutliff, P. Thayer, M. J. Bortner, E. J. Foster, *Front Bioeng Biotechnol* **2019**, *7*.

[4] R. A. Buswell, W. R. Leal de Silva, S. Z. Jones, J. Dirrenberger, *Cem Concr Res* **2018**, *112*, 37.

[5] Z. Zheng, D. Eglin, M. Alini, G. R. Richards, L. Qin, Y. Lai, *Engineering* **2021**, *7*, 966.

[6] J. Shi, B. Wu, S. Li, J. Song, B. Song, W. F. Lu, *Biomed Phys Eng Express* **2018**, *4*.

[7] W. Li, M. Wang, H. Ma, F. A. Chapa-Villarreal, A. O. Lobo, Y. S. Zhang, *iScience* **2023**, *26*, 106039.

[8] Z. Zheng, D. Eglin, M. Alini, G. R. Richards, L. Qin, Y. Lai, *Engineering* **2020**.

[9] Z. Yazdanpanah, J. D. Johnston, D. M. L. Cooper, X. Chen, *Front Bioeng Biotechnol* **2022**, *10*, 418.

[10] W. Li, L. S. Mille, J. A. Robledo, T. Uribe, V. Huerta, Y. S. Zhang, *Adv Healthc Mater* **2020**, *9*, 2000156.

[11] J. K. Placone, J. Navarro, G. W. Laslo, M. J. Lerman, A. R. Gabard, G. J. Herendeen, E. E. Falco, S. Tomblyn, L. Burnett, J. P. Fisher, *Ann Biomed Eng* **2017**, *45*, 237.

[12] X. Mu, F. Agostinacchio, N. Xiang, Y. Pei, Y. Khan, C. Guo, P. Cebe, A. Motta, D. L. Kaplan, *Prog Polym Sci* **2021**, *115*, 101375.

[13] X. Mu, J. K. Sahoo, P. Cebe, D. L. Kaplan, *Polymers (Basel)* **2020**, *12*, 1.

[14] A. Bahar, R. Rusijono, N. Kusumawati, **2018**, *171*, 46.

[15] S. Petros, T. Tesfaye, M. Ayele, *Journal of Engineering (United Kingdom)* **2020**, *2020*.

[16] S. CHATTERJEE, P. Chi-leung HUI, *Molecules* **2019**, *24*, 2547.

[17] K. Chen, Y. Feng, Y. Zhang, L. Yu, X. Hao, F. Shao, Z. Dou, C. An, Z. Zhuang, Y. Luo, Y. Wang, J. Wu, P. Ji, T. Chen, H. Wang, *ACS Appl Mater Interfaces* **2019**, *11*, 36458.

[18] Y. Wang, M. Ma, J. Wang, W. Zhang, W. Lu, Y. Gao, B. Zhang, Y. Guo, *Materials 2018, Vol. 11, Page 1345* **2018**, *11*, 1345.

[19] A. A. Pawar, G. Saada, I. Cooperstein, L. Larush, J. A. Jackman, S. R. Tabaei, N.-J. Cho, S. Magdassi, *Sci Adv* **2016**, *2*, 1.

[20] Q. Ge, Z. Chen, J. Cheng, B. Zhang, Y. F. Zhang, H. Li, X. He, C. Yuan, J. Liu, S. Magdassi, S. Qu, *Sci Adv* **2021**, *7*, 1.

[21] X. Mu, F. Agostinacchio, N. Xiang, Y. Pei, Y. Khan, C. Guo, P. Cebe, A. Motta, D. L. Kaplan, *Prog Polym Sci* **2021**, *115*, 101375.

[22] C. M. Elvin, T. Vuocolo, A. G. Brownlee, L. Sando, M. G. Huson, N. E. Liyou, P. R. Stockwell, R. E. Lyons, M. Kim, G. A. Edwards, G. Johnson, G. A. McFarland, J. A. M. Ramshaw, J. A. Werkmeister, *Biomaterials* **2010**, *31*, 8323.

[23] P. G. Parsons, P. Goss, *Australian Journal of Experimental Biology and Medical Science* **1978**, *56*, 287.

[24] K. S. Lim, R. Levato, P. F. Costa, M. D. Castilho, C. R. Alcala-Orozco, K. M. A. Van Dorenmalen, F. P. W. Melchels, D. Gawlitta, G. J. Hooper, J. Malda, T. B. F. Woodfield, *Biofabrication* **2018**, *10*.

[25] D. Kam, A. Olender, A. Rudich, Y. Kan-Tor, A. Buxboim, O. Shoseyov, S. Magdassi, *Adv Funct Mater* **2022**, *2210993*.

[26] M. Xie, L. Lian, X. Mu, Z. Luo, C. E. Garciamendez-Mijares, Z. Zhang, A. López, J. Manríquez, X. Kuang, J. Wu, J. K. Sahoo, F. Z. González, G. Li, G. Tang, S. Maharjan, J. Guo, D. L. Kaplan, Y. S. Zhang, *Nat Commun* **2023**, *14*.

[27] D. Shin, J. Hyun, *Journal of Industrial and Engineering Chemistry* **2021**, *95*, 126.

[28] B. G. Soliman, A. Longoni, M. Wang, W. Li, P. N. Bernal, A. Cianciosi, G. C. J. Lindberg, J. Malda, J. Groll, T. Jungst, R. Levato, J. Rnjak-Kovacina, T. B. F. Woodfield, Y. S. Zhang, K. S. Lim, *Adv Funct Mater* **2023**, *33*.

[29] M. Krishani, W. Y. Shin, H. Suhaimi, N. S. Sambudi, *Gels* **2023**, *9*.

[30] X. Zhao, D. A. Hu, D. Wu, F. He, H. Wang, L. Huang, D. Shi, Q. Liu, N. Ni, M. Pakvasa, Y. Zhang, K. Fu, K. H. Qin, A. J. Li, O. Hagag, E. J. Wang, M. Sabharwal, W. Wagstaff, R. R. Reid, M. J. Lee, J. M. Wolf, M. El Dafrawy, K. Hynes, J. Strelzow, S. H. Ho, T. C. He, A. Athiviraham, *Front Bioeng Biotechnol* **2021**, *9*, 1.

[31] M. Chen, Z. Jiang, X. Zou, X. You, Z. Cai, J. Huang, *Heliyon* **2024**, *10*, e25400.

[32] M. Dufaud, L. Solé, M. Maumus, M. Simon, E. Perrier-Groult, G. Subra, C. Jorgensen, D. Noël, *Bioprinting* **2022**, *28*, e00253.

[33] M. J. Stoddart, E. Della Bella, A. R. Armiento, In *Methods in Molecular Biology*, **2022**, pp. 1–7.

[34] S. Landau, A. A. Szklanny, M. Machour, B. Kaplan, Y. Shandalov, I. Redenski, M. Beckerman, O. Harari-Steinberg, J. Zavin, O. Karni-Katovitch, I. Goldfracht, I. Michael, S. D. Waldman, S. I. Duvdevani, S. Levenberg, *Biofabrication* **2022**, *14*.

[35] J. Kundu, J.-H. Shim, J. Jang, S.-W. Kim, D.-W. Cho, *J Tissue Eng Regen Med* **2013**, *9*, 1286.

[36] A. Kosik-Kozioł, M. Costantini, A. Mróz, J. Idaszek, M. Heljak, J. Jaroszewicz, E. Kijeńska, K. Szöke, N. Frerker, A. Barbetta, J. E. Brinchmann, W. Święszkowski, *Biofabrication* **2019**, *11*.

[37] A. O., C. Crowley, M. Z., P. E., A. M., In *Tissue Engineering for Tissue and Organ Regeneration*, InTech, **2011**.

[38] H. Hong, Y. B. Seo, D. Y. Kim, J. S. Lee, Y. J. Lee, H. Lee, O. Ajiteru, M. T. Sultan, O. J. Lee, S. H. Kim, C. H. Park, *Biomaterials* **2020**, *232*, 119679.

[39] C. Lu, K. Deng, A. Porter, K. (Kelvin) Fu, *Adv Compos Hybrid Mater* **2023**, *6*, 1.

[40] X. Jiang, S. Lyu, M. Ali, J. Huang, W. Jiang, Z. Qiu, Q. Sui, *Water Science and Technology* **2020**, *82*, 998.

[41] P. F. Jacobs, *J Manuf Syst* **1993**, *12*, 430.

[42] P. F. Jacobs, *J Manuf Syst* **1993**, *12*, 430.

[43] Y. Ma, W. Wei, L. Gong, C. Li, Y. Hong, X. Wang, R. Liang, Q. Shao, Q. Liang, W. Huang, M. J. Shipston, H. Ouyang, *Cell Rep Phys Sci* **2022**, *3*, 100985.

[44] M. Leulescu, A. Rotaru, I. Pălărie, A. Moanţă, N. Cioateră, M. Popescu, E. Morîntale, M. V. Bubulică, G. Florian, A. Hărăbor, P. Rotaru, *J Therm Anal Calorim* **2018**, *134*, 209.

[45] GMIA, *Gelatin handbook*, **2019**.

[46] C. Chen, M. Zhang, A. S. Mujumdar, P. Phuhongsung, *Food Research International* **2021**, *148*, 110630.

[47] A. F. Ghazal, M. Zhang, B. Bhandari, H. Chen, *Food Research International* **2021**, *142*, 110215.

[48] F. Tsegay, M. Hisham, M. Elsherif, A. Schiffer, H. Butt, *Molecules* **2023**, *28*, 1.

[49] A. Kostelnik, A. Cegan, M. Pohanka, *Sensors (Switzerland)* **2016**, *16*.

[50] K. O. Rojek, M. Ćwiklińska, J. Kuczak, J. Guzowski, *Chem Rev* **2022**, *122*, 16839.

[51] M. B. Łabowska, M. Skrodzka, H. Sicińska, I. Michalak, J. Detyna, *Gels* **2023**, *9*.

[52] W. C. Luo, A. O'Reilly Beringhs, R. Kim, W. Zhang, S. M. Patel, R. H. Bogner, X. Lu, *European Journal of Pharmaceutics and Biopharmaceutics* **2021**, *169*, 256.

[53] M. Tsukamoto, T. Okuda, H. Okamoto, Y. Higuchi, S. Kawakami, F. Yamashita, M. Hashida, *Biol Pharm Bull* **2012**, *35*, 1178.

DLP printing of non-modified protein-only compositions

Ayelet Bunin[+], Orit Harari-Steinberg[+], Doron Kam, Tatyana Kuperman, Moran Friedman-Gohas, Bruria Shalmon, Liraz Larush, Shay I. Duvdevani[+], Shlomo Magdassi**

This research explores non-modified, protein-only bio-inks for digital light processing (DLP) printing. By harnessing the native gelatin properties, intricate 3D structures are fabricated. Visible light-induced crosslinking enables the fabrication of cell-laden and cell-seeded cartilage implants.